Induced-charge electrokinetics in a conducting nanochannel with broken geometric symmetry: Towards a flexible control of ionic transport

Cunlu Zhao, Yongxin Song, and Chun Yang

Citation: Physics of Fluids (1994-present) **27**, 012003 (2015); doi: 10.1063/1.4906773
View online: http://dx.doi.org/10.1063/1.4906773
View Table of Contents: http://scitation.aip.org/content/aip/journal/pof2/27/1?ver=pdfcov
Published by the AIP Publishing

PHYSICS OF FLUIDS **27**, 012003 (2015)

Induced-charge electrokinetics in a conducting nanochannel with broken geometric symmetry: Towards a flexible control of ionic transport

Cunlu Zhao,[1,a)] Yongxin Song,[2] and Chun Yang[1,b)]
[1]*School of Mechanical and Aerospace Engineering, Nanyang Technological University, Singapore*
[2]*Department of Marine Engineering, Dalian Maritime University, Dalian, Liaoning, China*

(Received 6 September 2014; accepted 13 January 2015; published online 28 January 2015)

In the literature, conventional electrokinetics is widely used as a principle of operating nanofluidic devices. Different from the conventional electrokinetics involving nonpolarizable solid surfaces with fixed surface charge, induced-charge electrokinetic (ICEK) phenomena deal with polarizable surfaces with the ability of surface charge modulation through electric polarization under external electric fields. Because of several advantages, ICEK phenomena have drawn a great deal of attention in microfluidic community. Herein, we propose the first effort of extending the ICEK phenomena from microfluidics to nanofluidics. In particular, we report a numerical model for the ICEK phenomena in a tapered nanochannel with conducting (ideally polarizable) walls. It is shown that due to the broken geometric symmetry of the nanochannel, induced-charge electroosmotic flow inside the nanochannel exhibits a flow rectification such that electrolyte solution always flows from the narrow end of the nanochannel to the wide end for either a forward electric bias (electric field from the narrow to wide ends) or a reverse electric bias (electric field from the wide to narrow ends). In addition, we demonstrate that the ion selectivity of such tapered conducting nanochannel can be actively tuned to be cation-selective with a forward bias and anion-selective with a reverse bias. Promisingly, conducting nanochannels with broken geometric symmetry could be potentially used for constructing nanofluidic pumps with the unidirectional pumping capacity and ion selectors with the tuneable ionic selection. [http://dx.doi.org/10.1063/1.4906773]

I. INTRODUCTION

Nanofluidics is of growing scientific and practical interests with various newly induced phenomena and a broad range of potential applications, such as transport, separation and detection of ions and biomolecules, and energy conversion, etc.[1–5] Typically, in nanofluidics at least one dimension of the fluidic channel (h) becomes comparable to or even smaller than the Debye length (κ^{-1}) which gives an estimation of the thickness of electric double layer (EDL) and usually ranges from 1 to 300 nm. Because of the overlap of EDLs ($\kappa h \ll 1$), counterions predominate inside the channel to neutralize the surface charge on channel walls.[6] The change of surface charge on channel wall breaks up the electric neutrality, and hence, the quantity of ions and/or the charge density inside the channel must change accordingly to regain the electroneutrality of the system. Consequently, modulation of the surface charge has been shown an effective way for manipulating the ionic transport inside nanochannels.[7,8] Generally, there are two established ways to control the surface charge.[6,9,10] For an insulating (nonpolarizable) surface, its surface charge is not affected by external electric field and can only be passively controlled by solution and surface physicochemical properties such as the

a)Current address: Physics of Complex Fluids, Faculty of Science and Technology, University of Twente, P.O. Box 217, 7500 AE Enschede, The Netherlands.
b)E-mail: mcyang@ntu.edu.sg

density/composition of chemical groups on the solid surface and the pH/ionic concentration of the bulk solution.[11–13] On the other hand, for an electrically conducting surface, its surface charge can be actively controlled by directly imposing electrical potential differences between the surface and the bulk electrolyte solution.[14–17]

In literature, the recently developed induced-charge electrokinetic (ICEK) phenomena arising from electrically polarizable surfaces provide a new means for modulating the surface charge in nanofluidics. The electric polarization of an initially uncharged conductor (assumed to be ideally polarizable) floating in external electric field can induce surface charge on the conductor and thus alter the EDL in an electrolyte solution surrounding the conductor. Generally, changes in the strength of external electric fields and/or the geometry of conductor would modify electric polarization of the conductor and hence the surface charge. Initially, the ICEK phenomena were reported in the colloid science community with focus on theoretical and experimental investigations of flow field around polarized colloidal particles in presence of external electric field.[18,19] Recently, Bazant and his collaborators[20–22] revisited ICEK phenomena with emphasis on microfluidic applications. Realizing the previous discussion of ICEK phenomena limited to surfaces with extreme electric properties (either highly conducting-conductors or non-conducting-insulators), Zhao and Yang[23,24] derived generalized electrokinetic boundary conditions for the prediction of induced zeta potentials in ICEK phenomena over solid surfaces with arbitrary electric properties. So far, ICEK phenomena have been successfully adopted to fulfil a number of microfluidic applications, such as pumping,[25–27] demixing,[28] mixing,[29–31] focusing,[32–34] and particle manipulations.[35,36]

Despite many theoretical and experimental studies of ICEK phenomena in microfluidics, we are not aware of any studies implementing the ICEK technique into nanofluidics. This paper thus reports the first use of ICEK phenomena in nanofluidics as a new means of surface charge modulation to control the ion transport and fluid flow. To be more specific, we report a numerical analysis of ICEK phenomena inside a tapered conducting nanochannel whose surface charge can be actively modulated by varying the applied electric field and taper angle of the channel walls. Our study shows that the broken geometric symmetry of the nanochannel (tapered nanochannel) enables ICEK phenomena to be a new and easy strategy of surface charge modulation for the active control of both ionic transport and liquid flow in nanofluidic channels. The use of tapered nanochannel in our study is motivated not only by the growing interests in utilizing asymmetric nanochannels or conical nanopores for transport of ions,[37–43] but also by the fact that the asymmetry of channel is a prerequisite for the ICEK mechanism to function in the nanofluidic system.

II. THE NANOCHANNEL SYSTEM AND GOVERNING EQUATIONS OF ICEK PHENOMENA

We consider a two dimensional tapered nanochannel with a length L, a height of right opening $2h_2$, and a height of left opening $2h_1$, as shown in Figure 1. The conducting nanochannel can be

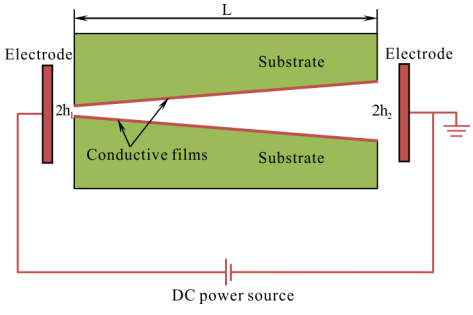

FIG. 1. Schematic of our nanofluidic system with a conducting tapered nanochannel. The tapered nanochannel can be formed with two insulating substrates first, and then the walls can become conducting by coating with conductive (ideally polarizable) films. The length of the tapered nanochannel is L, the height of the left opening of the channel is $2h_1$, and the height of the right opening is $2h_2$. A power source is used to setup an external driving electric field for driving fluid flow inside the nanochannel. The right electrode is grounded, and the driving electric field can be adjusted by varying the applied voltage on the left electrode, φ_0. The conducting nanochannel walls are polarized upon turning on the external driving electric field.

fabricated with multiple standard techniques developed in micro/nano fabrication, with first the nanochannel formed in an insulating or low-conductivity substrate (e.g., silicon) using an etching process and then the nanochannel wall coated with good conducting materials (e.g., diamond-like carbon or Au) using a sputtering process.[14,44,45] The right electrode is grounded, and the potential on the left electrode denoted by φ_0 is adjustable by a DC power source. The conducting nanochannel walls floating in the external driving electric field are polarized to acquire surface charge which can play the same roles as physicochemical surface charge in the traditional electrokinetics.[6,20,21] At each opening, the nanochannel is connected to a reservoir containing an electrolyte (e.g., KCl solution) with a bulk concentration, c_0. For simplicity, the bulk concentrations in both reservoirs are assumed to be the same.

At first, we nondimensionalize the governing equations that describe the ICEK phenomena in the nanofluidic system by introducing the following reference quantities for electric potential, velocity, pressure, electric current density, electric current, and surface charge density, respectively, as

$$\varphi_{ref} = \frac{RT}{F},\ u_{ref} = \frac{\varepsilon_0\varepsilon_r\varphi_{ref}^2}{\mu L_{ref}},\ p_{ref} = \mu\frac{u_{ref}}{L_{ref}},\ i_{ref} = Fu_{ref}c_{ref},$$
$$I_{ref} = Fu_{ref}c_{ref}L_{ref},\ q_{ref} = \varepsilon_0\varepsilon_r\frac{\varphi_{ref}}{L_{ref}}, \tag{1}$$

as well as the Reynolds number for the liquid flow and the Peclet number for the ionic species transport,

$$Re = \frac{\rho u_{ref}L_{ref}}{\mu},\ Pe = \frac{u_{ref}L_{ref}}{D_{ref}}, \tag{2}$$

where L_{ref}, c_{ref}, and D_{ref} denote the reference length scale, the reference ionic concentration, and the reference ionic diffusion coefficient, respectively, and all of them are to be specified in Sec. III. φ_{ref} is the so-called thermal voltage with a value of 25.7 mV at room temperature. In Eqs. (1) and (2), F is the Faraday constant, R is the universal gas constant, T is the absolute temperature, ε_0 represents the permittivity of vacuum, and ε_r, ρ, and μ are the dielectric constant, density, and dynamic viscosity of the electrolyte solution, respectively.

The local electric potential and net charge density are related by the Poisson equation which can be expressed in nondimensional form as

$$\nabla^2\varphi = -\frac{1}{2}(\kappa L_{ref})^2\sum_{j=1,2} z_j c_j, \tag{3}$$

where φ is the dimensionless electric potential, c_j is the dimensionless concentration of ions in the electrolyte solution, z_j is the valence of the ions, with subscript $j = 1$ (2) corresponding to cations (anions), and κ is the inverse of Debye length given by $\kappa = \sqrt{(2c_{ref}F^2)/(\varepsilon_0\varepsilon_r RT)}$.

At the steady state, the local concentration of ionic species in the electrolyte solution is governed by the dimensionless Nernst-Planck equation

$$Pe\,(\mathbf{u}\cdot\nabla c_j) = D_j\nabla^2 c_j + D_j z_j\nabla\cdot(c_j\nabla\varphi), \tag{4}$$

where $\mathbf{u}$ is the velocity vector and it has two components (u, v) in x direction and y direction, respectively, and D_j denotes the normalized diffusion coefficient for ionic species.

The motion of electrolyte solution is governed by the continuity and Navier–Stokes equations

$$\nabla\cdot\mathbf{u} = 0, \tag{5a}$$

$$Re\,(\mathbf{u}\cdot\nabla\mathbf{u}) = -\nabla p + \nabla^2\mathbf{u} - \frac{1}{2}(\kappa L_{ref})^2\nabla\varphi\sum_{j=1,2} z_j c_j, \tag{5b}$$

where p is the dimensionless pressure, and the third term on the right hand side of Eq. (5b) represents the electrostatic body force due to the non-electroneutrality in the electrolyte solution. Although the liquid flow in nanofluidics is dominated by viscous effects because of very small

Reynolds numbers, the convective transport of momentum in Eq. (5b) is still retained for completeness.

The electric current for species j can be obtained by integrating the current density over the cross section of the nanochannel

$$I_j = \int_{s_1} i_{j,x} ds_1, \tag{6}$$

where s_1 is the surface element of the nanochannel cross-section, $i_{j,x}$ denotes the x component of the current density vector for the ion species j, $\boldsymbol{i}_j$, which can be expressed as

$$\boldsymbol{i}_j = \mathbf{u} z_j c_j - \frac{1}{Pe} z_j D_j \nabla c_j - \frac{\nabla \varphi}{Pe} z_j^2 D_j c_j. \tag{7}$$

The ionic selectivity of tapered conducting nanochannels is defined in a similar fashion to that used in insulating nanochannels[10,46]

$$S = \frac{|I_1| - |I_2|}{|I_1| + |I_2|} \tag{8}$$

which ranges from −1 to 1. The selectivity defines a preference for particular ions to be transported. When S is in the range of (−1, 0), the channel shows anion selective function, while when S is in the range of (0, 1), the channel shows cation selective function. Ideally, $S = 1$ (−1) indicates a perfectly cation (anion) selective nanochannel and $S = 0$ would correspond to a nonselective nanochannel.

III. DESCRIPTION OF THE SIMULATED DOMAIN AND BOUNDARY CONDITIONS

Since the entire tapered nanofluidic system is symmetric with respect to the channel axis, only the lower half of the system including the reservoirs and the nanochannel is simulated as sketched in Figure 2. The solution is symmetric electrolyte KCl with $z_1 = -z_2 = 1$. The reference ionic diffusion coefficient D_{ref} is chosen as 10^{-9} m^2/s, and then at room temperature (T = 298 K), the normalised ionic diffusion coefficients for two ionic species are $D_1 = 1.957$ and $D_2 = 2.032$.[47] Then we can calculate that $Pe = 5.10 \times 10^{-1}$ and $Re = 5.66 \times 10^{-4}$. Furthermore, c_{ref} is set to be the bulk ionic concentration inside the reservoirs, c_0, and L_{ref} is chosen as the half height of the right opening h_2. In all the simulations, we set $L/h_2 = 200$ and the electrokinetic parameter $\kappa L_{ref} = \kappa h_2 = 1$, which ensures that the channel dimension is comparable to the thickness of EDL and is in nanometre scale. These nondimensional values of L/h_2 and κh_2 together with $h_1/h_2 = 0.2$ typically represent a nanochannel system with geometric dimensions of $2h_1 = 6$ nm, $2h_2 = 30$ nm, and $L = 3$ μm and a bulk ionic concentration of $c_0 = 4.1 \times 10^{-4}$ M in two reservoirs. The advantage of using nondimensional parameters in the investigation is that for a given value of κh_2, there is a combination of many different values of c_0 and h_2. Therefore, for $\kappa h_2 = 1$, it also could represent the cases with the bulk concentration of $c_0 = 4.1$ mM ($c_0 = 41$ mM) and $2h_2 = 9.5$ nm ($2h_2 = 3$ nm).

To complete the formulation, the relevant boundary conditions must be specified on the boundaries sketched in Figure 2 for the Poisson, Nernst-Planck, and Navier-Stokes equations, and they are summarised in Table I. Symmetric boundary conditions for three governing equations are applied along the symmetric boundary AH. Along the boundary AB, the electric potential is set to be φ_0 which is adjustable by the DC power source in Figure 1. The boundary GH is taken as the

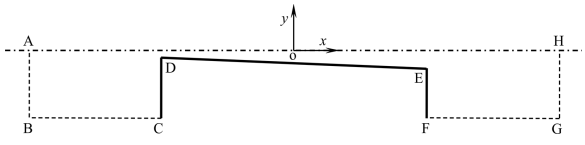

FIG. 2. The sketch of the simulated domain. The Cartesian coordinates (x, y) are normalised with respect to the half-height of right opening h_2.

TABLE I. Boundary conditions for the numerical solutions of the Poisson equation, the Nernst-Planck equation, and the Navier-Stokes equation in the computational domain sketched in Figure 2.

Boundary segments	Poisson equation	Nernst–Planck equation	Navier–Stokes equation
AB	Specified potential $\varphi = \varphi_0$	Bulk ionic concentrations $c_j = 1$	Zero normal pressure $p = 0$
BC, FG	No charge $\mathbf{n} \cdot \nabla\varphi = 0$	No normal flux $\mathbf{n} \cdot \left(\mathbf{u}c_j - D_j\nabla c_j/Pe - D_j z_j c_j \nabla\varphi/Pe\right) = 0$	Slip $\mathbf{n} \cdot \mathbf{u} = 0$
CD, EF	No charge $\mathbf{n} \cdot \nabla\varphi = 0$	No normal flux $\mathbf{n} \cdot \left(\mathbf{u}c_j - D_j\nabla c_j/Pe - D_j z_j c_j \nabla\varphi/Pe\right) = 0$	No slip $\mathbf{u} = 0$
DE	Floating boundary $\int_s (\mathbf{n} \cdot \nabla\varphi)\, ds = Q$	No normal flux $\mathbf{n} \cdot \left(\mathbf{u}c_j - D_j\nabla c_j/Pe - D_j z_j c_j \nabla\varphi/Pe\right) = 0$	No slip $\mathbf{u} = 0$
GH	Ground $\varphi = 0$	Bulk ionic concentrations $c_j = 1$	Zero normal pressure $p = 0$
AH	Symmetric boundary $\mathbf{n} \cdot \nabla\varphi = 0$	Symmetric boundary $\mathbf{n} \cdot \left(\mathbf{u}c_j - D_j\nabla c_j/Pe - D_j z_j c_j \nabla\varphi/Pe\right) = 0$	Symmetric boundary $\mathbf{n} \cdot \mathbf{u} = 0$

potential reference (i.e., grounded as shown in Figure 1). All walls of the reservoirs are assumed to be uncharged. DE is the conducting wall of the nanochannel that is floating in the electric field set up by the two driving electrodes inside two reservoirs. As a consequence, the electric field polarizes the conducting walls and causes redistribution of the surface charge on them. There is no charge exchange between conducting walls and their surroundings since conducting walls are ideally polarizable. Then the floating boundary condition[48] which constrains the total charge on the conducting surface is used along boundary DE. In the floating boundary condition tabulated in Table I, Q is the overall dimensionless free surface charges acquired by the conducting surface due to the physicochemical mechanism before applying the external electric field, and s stands for the surface element for the boundary DE and is normalised with respect to L_{ref}. The non-dimensional Q is obtained by normalising the overall free surface charges with respect to $\varepsilon_0\varepsilon_r\varphi_{ref}$. Since our focus is placed on induced charge electrokinetic flow, for simplicity, $Q = 0$ is used in the present work due to the assumption of initially uncharged conducting walls of the nanochannel (i.e., physicochemical mechanisms in the conventional electrokinetics do not contribute to any surface charge in ICEK phenomena).

Boundaries AB and GH are the bulk reservoir and the concentrations of the positive and negative ions are the same as that of the bulk electrolyte in the reservoirs. Electrolyte ions cannot penetrate through the solid surfaces, so the net ionic fluxes normal to the walls of the reservoirs and the nanochannel (boundaries CD, DE, EF, BC, and FG) vanish.

Finally, in order to solve the hydrodynamic problem governed by Eqs. (5a) and (5b), nonslip boundary conditions are specified on the solid walls of nanochannel and reservoirs (boundaries CD, DE, and EF). Normal pressure $p = 0$ is used on the boundaries AB and GH due to no applied pressure difference between two reservoirs. Finally, slip boundary conditions are applied on boundaries BC and FG which are away from the entrance and exit of the nanochannel. With the boundary conditions provided in Table I, the problem can be solved numerically.[49]

IV. RESULTS AND DISCUSSION

A. Electroosmosis in tapered nanochannels with floating conducting walls

Figure 3 depicts the electric potential and ionic concentrations along the centreline of nanochannel with floating conducting walls when the system is forwardly biased ($\varphi_0 = 6$) and reversely biased ($\varphi_0 = -6$) for $h_1/h_2 = 0.2$. For the forward bias situation in Figure 3(a), the electric potential decreases along the axial direction and two potential barriers exist at the two junctions connecting the nanochannel and the two reservoirs. Furthermore, the barrier at the narrow nanochannel-reservoir junction is more significant than that at the wide nanochannel-reservoir junction. It is also manifested that in the right half of the nanochannel, the concentration of the anions is slightly higher than that of the cations;

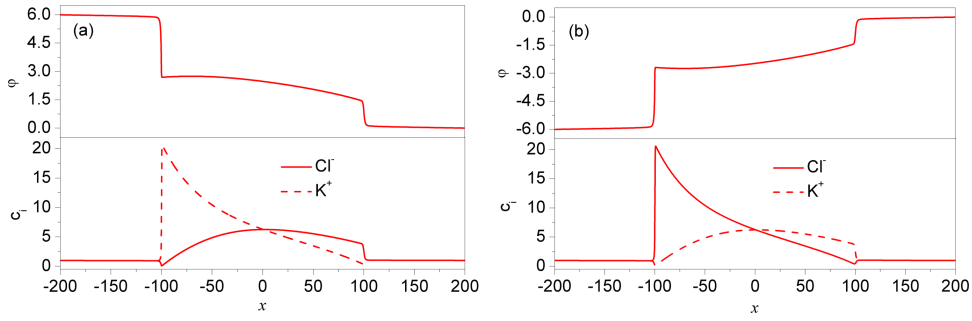

FIG. 3. Profiles of electric potential φ and ion concentration c along the axis of a tapered conducting nanochannel (y = 0) with $h_1/h_2 = 0.2$ for (a) the forward electric bias of $\varphi_0 = 6$ and (b) the reverse electric bias of $\varphi_0 = -6$.

while in the left half of the nanochannel, the concentration of the cations is significantly higher than that of the anions. In the middle section of the nanochannel, both the cations and anions have the same concentration. In the two reservoirs, the solution is electrically neural, and thus, the cations and anions are with the same scaled bulk concentration of unity. When the system is reversely biased (Figure 3(b)), the electric potential increases along the axial direction, and there are also two potential barriers at the junctions connecting the nanochannel and the two reservoirs. The ionic distributive characteristics inside the nanochannel can be obtained by simply interchanging the profiles of K^+ and Cl^- presented in Figure 3(a). The corresponding flow characteristics inside the nanochannel are presented in Figure 4. It is interesting to find that the flow characteristics under two electric biases of same magnitude but opposite polarities are identical. The pressure shown in Figure 4(a) increases steeply from zero to its maximum at the left nanochannel-reservoir junction and then nonlinearly decreases along the nanochannel to the bulk value of zero in the right reservoir. The inset gives the corresponding pressure gradient, $-\mathrm{d}p/\mathrm{d}x$, inside the nanochannel ($-100 \le x \le 100$). This inset indicates that the pressure gradient is the largest at the channel inlet, then gradually decreases in the left-half region of the channel, and nearly remains as a constant in the right-half region of the channel. Also the pressure drop within the inlet and outlet regions of the nanochannel is quite significant. As shown in Figure 4(b), the axial velocity component (u) is positive inside a much larger portion of channel domain and slightly becomes negative only near the conducting wall at the wide end of the channel. These features allow for producing a net flow which is always from the narrow end to the wide end, regardless of the polarities of applied electric biases.

Furthermore, the induced surface charge density on the conducting wall of the tapered nanochannel is shown in Figure 5, which sheds light on the physics involved in Figures 3 and 4. In Figure 5, the non-dimensional induced surface charge density is obtained by using $q = \mathbf{n} \cdot \nabla\varphi$ (where $\mathbf{n}$ is the outward normal of conducting wall) and the reference charge density $q_{\mathrm{ref}} = 1.19\ \mathrm{mC/m^2}$ (note that such reference value is calculated from Eq. (1) with the reference potential being thermal voltage (25.7 mV)

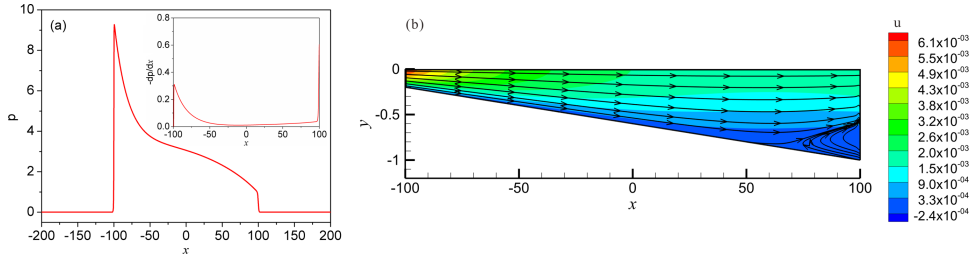

FIG. 4. Flow characteristics in a conducting tapered nanochannel with $h_1/h_2 = 0.2$ when the magnitude of electric bias $|\varphi_0| = 6$ (either forwardly biased or reversely biased). (a) The pressure p profile along the nanochannel axis (y = 0) and (b) the contour plot for the velocity component in the x direction, u. The inset in (a) shows the corresponding pressure gradient, $-\mathrm{d}p/\mathrm{d}x$, along the nanochannel axis.

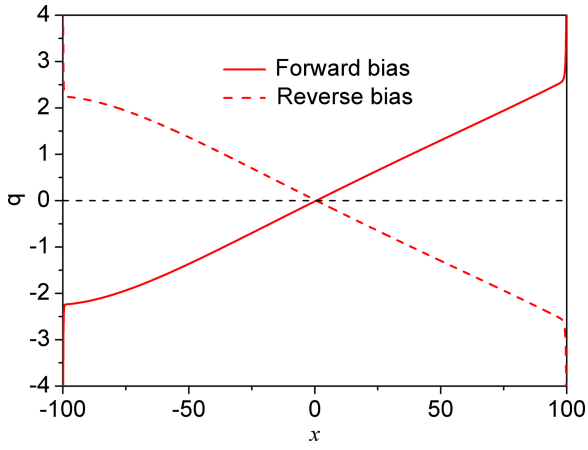

FIG. 5. The induced surface charged density q along the conducting wall due to the electric polarization for the forward bias of $\varphi_0 = 6$ and the reverse bias of $\varphi_0 = -6$ when $h_1/h_2 = 0.2$.

and the reference length h_2 being 15 nm). It can be seen that the conducting wall is half negatively polarized and half positively polarized for electric biases of both polarities. Generally, the induced surface charge density is distributed nonlinearly along x within the inlet region of the nanochannel (roughly $-100 \le x \le -50$) but stays linear in the rest of the nanochannel. Such nonlinearity at the nanochannel inlet is presumably due to the asymmetry of nanochannel. For symmetric nanochannels with $h_1 = h_2$, the surface charge density is rather linear inside the entire channel.[17] Evidently, the surface charge induced by electric polarization can play the roles in a similar fashion to the physicochemical bond surface charge in conventional electrokinetics. In other words, if the surface charge density depicted in Figure 5 is prescribed for the channel wall in the conventional electrokinetics, the resulting situation emulates the ICEK phenomena with the floating conducting wall of tapered nanochannel. Subsequently, the forward biased case is interpreted to unveil the mechanism of ICEK phenomena inside the tapered conducting nanochannel. Upon switching on the forward electric bias, the conducting nanochannel wall is instantaneously polarized with the right half of the wall surface acquiring positive charge and the left half of the wall acquiring negative charge. Then in order to neutralize such induced surface charge, in the solution domain, the anions predominate in the right half of the channel and the cations predominate in the left half of the channel. Due to the geometric asymmetry of the nanochannel, the resulting positive net charge density in the narrow left half of the nanochannel significantly outcompetes the negative net charge density in the wide right half of the nanochannel (see Figure 3(a)). The interactions of the external electric field with these two unequal charge densities inside two halves of the nanochannel give rise to a net body force which directs towards the positive x direction. Such net body force drives the liquid solution to move from the narrow end to the wide end. For the reversely biased situation, the polarization of the conducting wall reverses as shown in Figure 5, and so does the external electric field and the signs of net charge densities inside two halves of the nanochannel (see Figure 3(b)). Since the electric body force is a product of the electric field strength and the charge density, simultaneous reversion of the direction of electric field and the sign of charge density does not affect both the direction and magnitude of the net electric body force. Consequently, the same flow field as the forward bias should be expected.

B. Characteristics of ionic transport and liquid flow in tapered conducting nanochannels

Figure 6 presents the effect of electric bias on the ionic transport characteristics and the fluid flow rate. It is seen from Figure 6(a) that, although the total ionic current shows no rectification, the corresponding cationic and anionic currents do exhibit rectifying behaviours. To be more specific, the magnitude of cationic current for the forward bias is larger than that for the reserve bias, while the magnitude of anionic current for the forward bias is smaller than that for the reverse bias. It

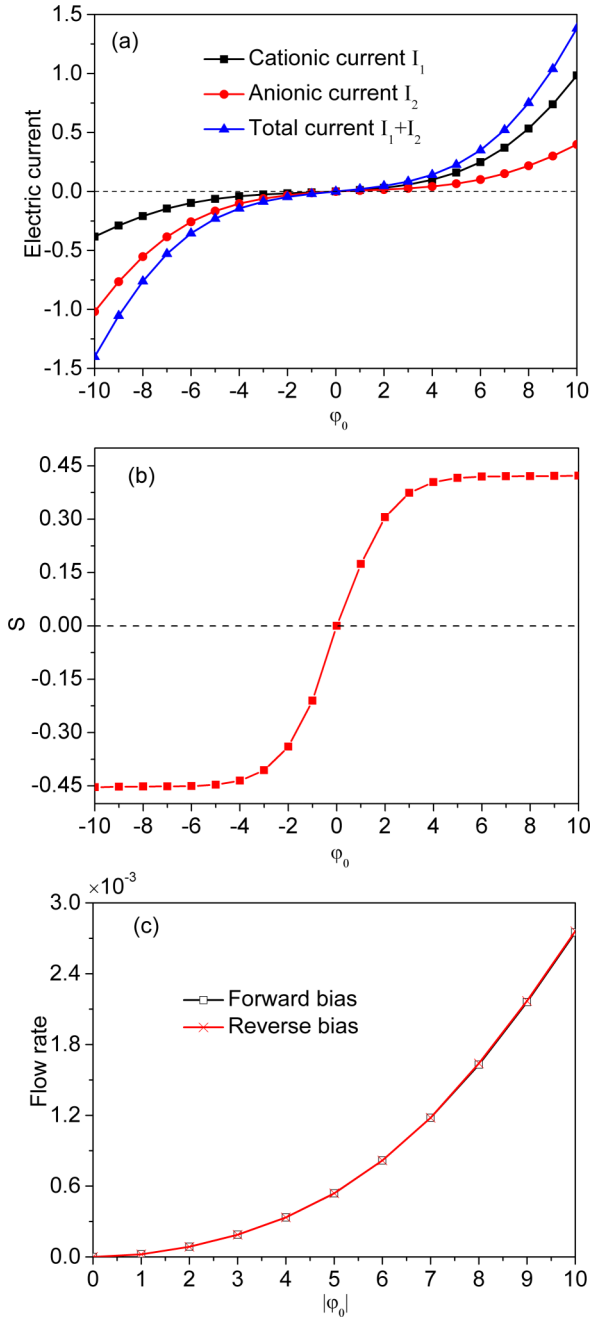

FIG. 6. Dependence of the ionic transport and flow rate on electric bias for a tapered nanochannel with $h_1/h_2 = 0.2$. (a) Variation of cationic, anionic, and total currents with electric bias. (b) Variation of the ionic selectivity, S, with electric bias. (c) Variation of the flow rate with electric bias.

should be noted that such ion transport is different from the conventional electrokinetics driven tapered nanopores or nanochannels which only show the total current rectification.[38,39,43] What is also identified from Figure 6(a) is that the cationic current is larger than the anionic current under the forwardly biased condition, which indicates a cation-selective behaviour, while the situation is completely opposite under the reversely biased condition where an anion-selective behaviour is observed. At last, to gain an in-depth quantitative understanding of ionic selective characteristics of the tapered nanochannel with conducting walls, the characteristics of ionic selectivity defined

in Eq. (8) are depicted in Figure 6(b). Generally, the tapered conducting nanochannel is nonselective when the bias is zero, cation-selective when it is forwardly biased, and anion-selective when it is reversely biased. At relatively low voltages, magnitudes of both anionic and cationic selectivity increase significantly with increasing the magnitude of applied electric bias. At high voltages (e.g., larger than 4), the magnitude of selectivity however increases very slowly and tends to saturation. This behaviour at large magnitudes of electric bias is reminiscent of the similar phenomena in the electrodialysis across membranes[50,51] where bulk concentration gradients (concentration polarization) were identified as the cause for such saturation behaviour. The details of concentration polarization inside two reservoirs are to be discussed in Sec. IV C. Figure 6(c) is the plot for the variation of scaled fluid flow rate through the nanochannel with the magnitude of the electric bias. As discussed earlier in this work, for the same magnitude of electric biases, the reversion of electric field direction does not affect the flow field, so reverse and forward biases with the same magnitude produce a same flow rate. It is also shown that the flow rate increases nonlinearly with an increase of the magnitude of electric biases. This intrinsic nonlinearity differentiates ICEK phenomena from conventional electrokinetic phenomena in which the flow rate is linearly proportional to the applied biases.

The effects of taper angle of the nanochannel on the ionic transport and the flow rate are presented in Figure 7. In the present analysis, while varying h_1/h_2, a fixed value of $L/h_2 = 200$ is used (also the channel length is fixed), and the smallest h_1/h_2 is chosen as 0.02. It is clear from Figure 7(a) that both cationic and anionic currents increase with the ratio of h_1/h_2. Also available from this plot is that the anionic current increases much faster than the cationic current. When h_1/h_2 is very close to unity, the anionic current slightly surpasses the cationic current. As long as the height of the left opening is not zero, with increasing h_1/h_2, the ionic selectivity (see Figure 7(b)) monotonically decreases, which can be readily explained by the characteristics of ionic currents depicted in Figure 7(a). When $h_1/h_2 = 1$ (straight nanochannels), the channel exhibits very weak anion-selective characteristics, which has been attributed to the larger diffusion coefficient of anions.[17] It also should be noted here that the selectivity becomes indefinite when $h_1/h_2 = 0$ since both denominator and numerator in Eq. (8) are zero. For the flow rate shown in Figure 7(c), it is clear that there exists an optimal height for the left opening at which the flow rate reaches the maximum value. In this particular case, the optimal height for the left opening is around $h_1 = 0.5h_2$. One inset in Figure 7(c) presents the axial velocity contour corresponding to $h_1 = 0.5h_2$, which is quite similar to the case of $h_1 = 0.2h_2$ in Figure 4(b). In spite of the decrement of the velocity magnitude for $h_1 = 0.5h_2$ as compared to $h_1 = 0.2h_2$, the increment of left opening of the channel from $h_1 = 0.2h_2$ to $h_1 = 0.5h_2$ is presumably dominant, thereby leading to a maximum volume flow rate at $h_1 = 0.5h_2$. When $h_1 < 0.5h_2$, the flow rate increases with an increase in h_1/h_2, while when $h_1 > 0.5h_2$, the flow rate decreases with an increase in h_1/h_2. At two extreme limits, i.e., $h_1/h_2 = 0$ and $h_1/h_2 = 1$, both net flow rates are zero. Specifically, another inset in Figure 7(c) shows that the zero flow rate for the straight channel case ($h_1 = h_2$) is a result of two symmetrical ICEK flow vortices inside the nanochannel.[17] Therefore, there is certainly a competition between the flow enhancement due to increasing h_1/h_2 and the flow reduction due to vortical flows. When $h_1 < 0.5h_2$, the flow enhancement due to increasing h_1/h_2 is more significant than the flow reduction caused by vortical flows, while when $h_1 > 0.5h_2$, the flow reduction due to vortical flows becomes dominant.

C. Concentration polarization inside the reservoirs

Another fundamental aspect of an ion-selective nanochannel is the generation of bulk electrolyte gradients, usually known as concentration polarization. Figure 8 shows the details of concentration polarization inside two reservoirs for various values of forward electric bias. It should be pointed out that only the electroneutral regions (with equal concentration of K^+ and Cl^+) are the bulk concentration polarization zones,[52,53] and the charged regions very near the nanochannel inlet and outlet are so-called space charge zones. The formation of these two zones inside the reservoirs is universal for ion-selective nanochannels or membranes. Thus, it would be expected that the ion-selective process in a conducting tapered nanochannel due to ICEK phenomena also induces two zones inside the reservoirs. For three cation-selective processes shown in Figure 8, the bulk

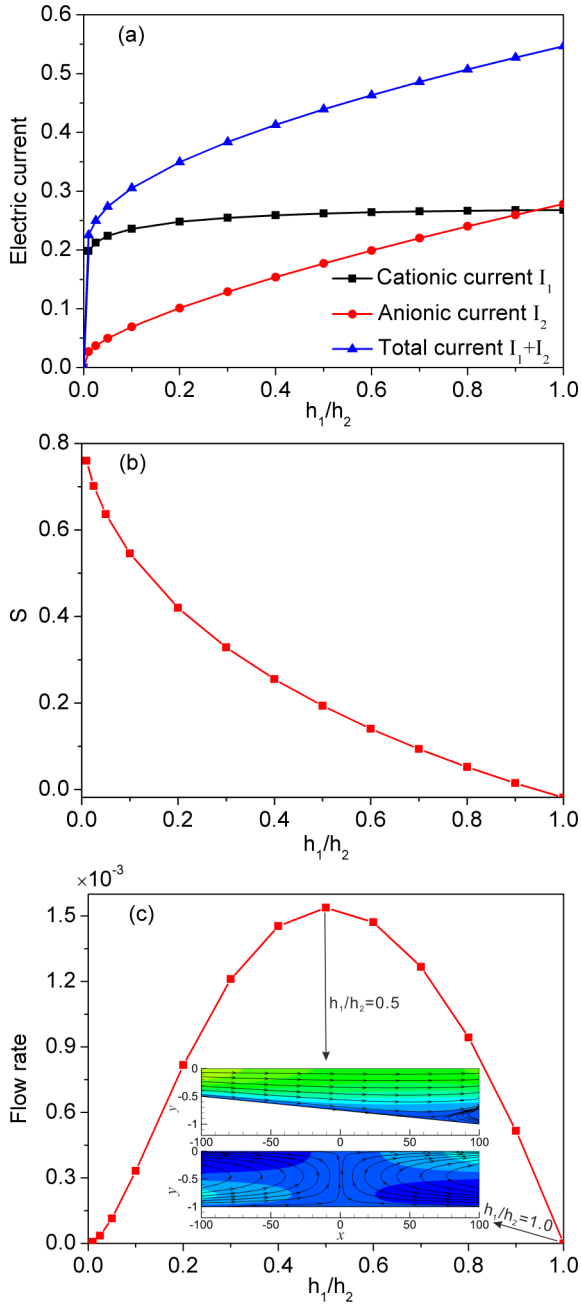

FIG. 7. Dependence of the ionic transport and flow rate on taper angle of the channel wall when $\varphi_0 = 6$. (a) Variation of cationic, anionic, and total currents with h_1/h_2. (b) Variation of the ionic selectivity, S, with h_1/h_2. (c) Variation of the flow rate with h_1/h_2. The plot (c) also includes two insets showing the contours of velocity field (axial component, u) for $h_1/h_2 = 0.5$ and 1.0. The arrowed lines in the two insets are streamlines, and the scale of velocity can be read from the contour legend of Figure 4(b).

electrolyte concentration decreases along the channel axis in both left and right reservoirs. These characteristics of concentration polarization are similar to those for cation-selective nanochannels driven by conventional electrokinetic phenomena (see Figure 18 in Ref. 2 and Figure 1 in Ref. 52). It is also evident from Figure 8 that the intensity of the concentration polarization increases with increasing the magnitude of electric bias, and also the space charge zone tends to occupy a much larger portion of the reservoir as the magnitude of electric bias increases. With a larger forward

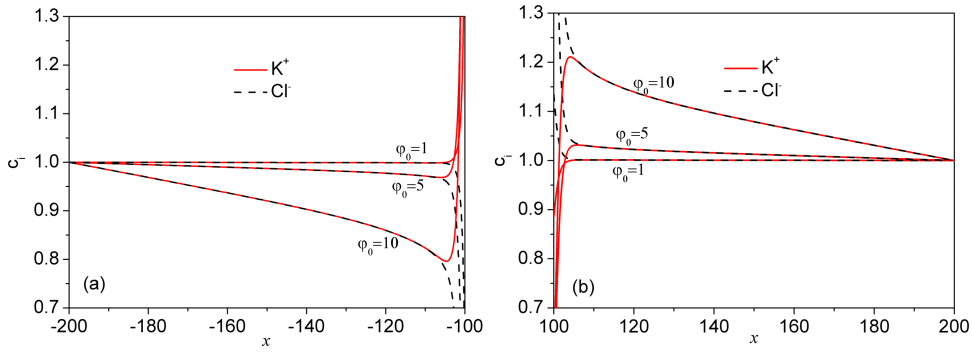

FIG. 8. Concentration polarization inside the two reservoirs for three different values of forward electric bias when $h_1/h_2 = 0.2$. (a) Ionic concentration profiles along the nanochannel axis (y = 0) inside the left (inlet) reservoir. (b) Ionic concentration profiles along the nanochannel axis (y = 0) inside the right (outlet) reservoir.

electric bias applied, preferential transfer of cations through the nanochannel would significantly deplete cations near the inlet of nanochannel in the left reservoir, so that a concentration gradient must form inside the bulk reservoir to maintain an appreciably lower concentration of electrolyte near the nanochannel inlet. Such change in the ionic concentration is equivalent to the reduction of the effective bulk concentration of electrolyte which manifests as a tendency for ionic selectivity saturation.[52] When the magnitude of electric bias is large enough to completely deplete both cations and anions near nanochannel inlet, the electric current reaches its high limiting value (so-called limiting current),[2] and thus the selectivity approaches its limit of saturation. In the present technique, ion-selective function is achieved by the ICEK technique in a conducting nanochannel. The high DC electric bias however would engender some negative effects in real applications, such as disruption of conducting films due to Faradaic reactions, which are beyond the scope of the present work. Therefore, limiting behaviours of concentration polarization and ionic selectivity at high voltages are not discussed here.

At last, it is also worthwhile discussing the effect of induced flow on the concentration polarization in Figure 8. Understandably, a stronger flow resulted from a stronger electric field (see Figure 6(c)) would convect more cations from the narrow end to the wide end of channel. Such effect certainly assists the depletion (enrichment) of cations inside the left (right) reservoir and thus intensifies the concentration polarization or the concentration gradient as well.

V. CONCLUSIONS

In this study, we proposed the implementation of the ICEK phenomena in nanofluidics for the first time. Specifically, we analyzed the ICEK phenomena in tapered conducting nanochannels and further identified it to be a brand-new method for flexible modulation of surface charge which governs ionic species transport inside the nanochannels. The detailed field information of ICEK phenomena in tapered conducting nanochannels was obtained by numerically solving the highly coupled Poisson, Nernst-Planck, and Navier-Stokes equations. The results revealed interesting characteristics for the fluid flow and the ionic transport induced by the ICEK phenomena in tapered conducting nanochannels: (i) for the liquid flow, the tapered conducting nanochannel demonstrates a flow rectification that the fluid always flows from the narrow end of the nanochannel to the wide end regardless the polarity of applied DC biases. It was also found that the flow rate increases monotonically and nonlinearly with increasing the magnitude of electric bias but attains the maximum value at an optimal taper angle of channel walls. (ii) For the ionic transport, although the total ionic current does not show any rectification, the corresponding cationic and anionic currents do exhibit rectifying characteristics, which make the nanochannel cation-selective when it is forward biased and anion-selective when it is reversely biased. Moreover, ionic selectivity increases monotonically with increasing the magnitudes of electric bias and/or taper angle of channel walls. Finally, it was identified that concentration polarization leads to the saturation of ionic selectivity at large electric

bias for tapered conducting nanochannels, which is similar to the ion transport across insulating ion-selective nanochannels or membranes by utilizing conventional electrokinetic phenomena.

In summary, tapered conducting nanochannels driven by the ICEK phenomena promise the flow rectification and the ionic selection, both of which can be dynamically and electrically controllable. Therefore, nanofluidic devices integrated with such tapered conducting nanochannels can be readily automated, thereby leading the controllability of nanofluidics to a much higher level.

ACKNOWLEDGMENTS

This work was supported by the Ministry of Education of Singapore under Grant No. RG93/14 and the University 111 project of China under Grant No. B08046. Z.C.L. was supported by Nanyang Technological University through a research assistantship.

[1] J. C. T. Eijkel and A. van den Berg, "Nanofluidics: What is it and what can we expect from it?," Microfluid. Nanofluid. **1**, 249 (2005).
[2] R. B. Schoch, J. Han, and P. Renaud, "Transport phenomena in nanofluidics," Rev. Mod. Phys. **80**, 839 (2008).
[3] M. L. Kovarik and S. C. Jacobson, "Nanofluidics in lab-on-a-chip devices," Anal. Chem. **81**, 7133 (2009).
[4] W. Sparreboom, A. van den Berg, and J. C. T. Eijkel, "Principles and applications of nanofluidic transport," Nat. Nanotechnol. **4**, 713 (2009).
[5] C. Duan and A. Majumdar, "Anomalous ion transport in 2-nm hydrophilic nanochannels," Nat. Nanotechnol. **5**, 848 (2010).
[6] C. Zhao and C. Yang, "Advances in electrokinetics and their applications in micro/nano fluidics," Microfluid. Nanofluid. **13**, 179 (2012).
[7] A. Plecis, R. B. Schoch, and P. Renaud, "Ionic transport phenomena in nanofluidics: Experimental and theoretical study of the exclusion-enrichment effect on a chip," Nano Lett. **5**, 1147 (2005).
[8] Y. Chen, Z. Ni, G. Wang, D. Xu, and D. Li, "Electroosmotic flow in nanotubes with high surface charge densities," Nano Lett. **8**, 42 (2007).
[9] R. Karnik, R. Fan, M. Yue, D. Li, P. Yang, and A. Majumdar, "Electrostatic control of ions and molecules in nanofluidic transistors," Nano Lett. **5**, 943 (2005).
[10] I. Vlassiouk, S. Smirnov, and Z. Siwy, "Nanofluidic ionic diodes: Comparison of analytical and numerical solutions," ACS Nano **2**, 1589 (2008).
[11] L.-J. Cheng and L. J. Guo, "Rectified ion transport through concentration gradient in homogeneous silica nanochannels," Nano Lett. **7**, 3165 (2007).
[12] L.-J. Cheng and L. J. Guo, "Ionic current rectification, breakdown, and switching in heterogeneous oxide nanofluidic devices," ACS Nano **3**, 575 (2009).
[13] M. X. Macrae, S. Blake, M. Mayer, and J. Yang, "Nanoscale ionic diodes with tunable and switchable rectifying behavior," J. Am. Chem. Soc. **132**, 1766 (2010).
[14] M. Nishizawa, V. P. Menon, and C. R. Martin, "Metal nanotubule membranes with electrochemically switchable ion-transport selectivity," Science **268**, 700 (1995).
[15] C.-C. Chang and R.-J. Yang, "Chaotic mixing in electro-osmotic flows driven by spatiotemporal surface charge modulation," Phys. Fluids **21**, 052004 (2009).
[16] E. Kalman, O. Sudre, I. Vlassiouk, and Z. Siwy, "Control of ionic transport through gated single conical nanopores," Anal. Bioanal.Chem. **394**, 413 (2009).
[17] C. Zhao and C. Yang, "Ion transport and selection through DCGC-based electroosmosis in a conducting nanofluidic channel," Microfluid. Nanofluid. (published online 2014).
[18] N. I. Gamayunov, V. A. Murtsovkin, and A. S. Dukhin, "Pair interaction of particles in electric field.1. Features of hydrodynamic interaction of polarized particles," Colloid J. USSR **48**, 197 (1986).
[19] V. A. Murtsovkin, "Nonlinear flows near polarized disperse particles," Colloid J. Russ. Acad.: Kolloidn. Zh. **58**, 341 (1996).
[20] M. Z. Bazant and T. M. Squires, "Induced-charge electrokinetic phenomena: Theory and microfluidic applications," Phys. Rev. Lett. **92**, 066101 (2004).
[21] T. M. Squires and M. Z. Bazant, "Induced-charge electro-osmosis," J. Fluid Mech. **509**, 217 (2004).
[22] M. Z. Bazant and T. M. Squires, "Induced-charge electrokinetic phenomena," Curr. Opin. Colloid Interface Sci. **15**, 203 (2010).
[23] C. Zhao and C. Yang, "AC field induced-charge electroosmosis over leaky dielectric blocks embedded in a microchannel," Electrophoresis **32**, 629 (2011).
[24] C. Zhao and C. Yang, "AC electrokinetic phenomena over semiconductive surfaces: Effective electric boundary conditions and their applications," Phys. Rev. E **83**, 066304 (2011).
[25] M. Z. Bazant and Y. Ben, "Theoretical prediction of fast 3D AC electro-osmotic pumps," Lab Chip **6**, 1455 (2006).
[26] M. M. Gregersen, F. Okkels, M. Z. Bazant, and H. Bruus, "Topology and shape optimization of induced-charge electro-osmotic micropumps," New J. Phys. **11**, 075019 (2009).
[27] C. Zhao and C. Yang, "Analysis of induced-charge electro-osmotic flow in a microchannel embedded with polarizable dielectric blocks," Phys. Rev. E **80**, 046312 (2009).
[28] F. C. Leinweber, J. C. T. Eijkel, J. G. Bomer, and A. Van Den Berg, "Continuous flow microfluidic demixing of electrolytes by induced charge electrokinetics in structured electrode arrays," Anal. Chem. **78**, 1425 (2006).
[29] H. Zhao and H. H. Bau, "Microfluidic chaotic stirrer utilizing induced-charge electro-osmosis," Phys. Rev. E **75**, 066217 (2007).

[30] Z. Wu and D. Li, "Micromixing using induced-charge electrokinetic flow," Electrochim. Acta **53**, 5827 (2008).
[31] Z. Wu and D. Li, "Mixing and flow regulating by induced-charge electrokinetic flow in a microchannel with a pair of conducting triangle hurdles," Microfluid. Nanofluid. **5**, 65 (2008).
[32] R. Dhopeshwarkar, D. Hlushkou, M. Nguyen, U. Tallarek, and R. M. Crooks, "Electrokinetics in microfluidic channels containing a floating electrode," J. Am. Chem. Soc. **130**, 10480 (2008).
[33] D. R. Laws, D. Hlushkou, R. K. Perdue, U. Tallarek, and R. M. Crooks, "Bipolar electrode focusing: Simultaneous concentration enrichment and separation in a microfluidic channel containing a bipolar electrode," Anal. Chem. **81**, 8923 (2009).
[34] R. K. Perdue, D. R. Laws, D. Hlushkou, U. Tallarek, and R. M. Crooks, "Bipolar electrode focusing: The effect of current and electric field on concentration enrichment," Anal. Chem. **81**, 10149 (2009).
[35] T. M. Squires and M. Z. Bazant, "Breaking symmetries in induced-charge electro-osmosis and electrophoresis," J. Fluid Mech. **560**, 65 (2006).
[36] S. Gangwal, O. J. Cayre, M. Z. Bazant, and O. D. Velev, "Induced-charge electrophoresis of metallodielectric particles," Phys. Rev. Lett. **100**, 058302 (2008).
[37] Z. Siwy, E. Heins, C. C. Harrell, P. Kohli, and C. R. Martin, "Conical-nanotube ion-current rectifiers: The role of surface charge," J. Am. Chem. Soc. **126**, 10850 (2004).
[38] I. Vlassiouk and Z. S. Siwy, "Nanofluidic diode," Nano Lett. **7**, 552 (2007).
[39] D. Constantin and Z. S. Siwy, "Poisson-Nernst-Planck model of ion current rectification through a nanofluidic diode," Phys. Rev. E **76**, 041202 (2007).
[40] H. S. White and A. Bund, "Ion current rectification at nanopores in glass membranes," Langmuir **24**, 2212 (2008).
[41] E. C. Yusko, R. An, and M. Mayer, "Electroosmotic flow can generate ion current rectification in nano- and micropores," ACS Nano **4**, 477 (2009).
[42] J. M. Perry, K. Zhou, Z. D. Harms, and S. C. Jacobson, "Ion transport in nanofluidic funnels," ACS Nano **4**, 3897 (2010).
[43] G. Nguyen, I. Vlassiouk, and Z. S. Siwy, "Comparison of bipolar and unipolar ionic diodes," Nanotechnology **21**, 265301 (2010).
[44] A. Evtukh, V. Litovchenko, M. Semenenko, O. Yilmazoglu, K. Mutamba, H. L. Hartnagel, and D. Pavlidis, "Formation of conducting nanochannels in diamond-like carbon films," Semicond. Sci. Technol. **21**, 1326 (2006).
[45] A. Piruska, S. P. Branagan, A. B. Minnis, Z. Wang, D. M. Cropek, J. V. Sweedler, and P. W. Bohn, "Electrokinetic control of fluid transport in gold-coated nanocapillary array membranes in hybrid nanofluidic–microfluidic devices," Lab Chip **10**, 1237 (2010).
[46] I. Vlassiouk, S. Smirnov, and Z. Siwy, "Ionic selectivity of single nanochannels," Nano Lett. **8**, 1978 (2008).
[47] J. H. Masliyah and S. Bhattacharjee, *Electrokinetic and Colloid Transport Phenomena* (Wiley-Interscience, Hoboken, N.J., 2006).
[48] J. A. Stratton, *Electromagnetic Theory* (McGraw-Hill, New York, 1941).
[49] See supplementary material at http://dx.doi.org/10.1063/1.4906773. The Poisson equation (3), the Nernst-Planck equation (4) and the Navier-Stokes equation (5) form a strongly coupled system. To numerically solve such a system, the finite element software package Comsol Multiphysics 4.3 was adopted in the present work. The Comsol model was validated with three bench-mark tests prior to calculations. The details of the numerical method and its validation are provided in the supplementary material.
[50] I. Rubinstein, "Effect of concentration polarization upon the valency-induced counterion selectivity of ion-exchange membranes," J. Chem. Soc., Faraday Trans. 2 **80**, 335 (1984).
[51] I. Rubinstein, "Theory of concentration polarization effects in electrodialysis on counter-ion selectivity of ion-exchange membranes with differing counter-ion distribution coefficients," J. Chem. Soc., Faraday Trans. **86**, 1857 (1990).
[52] S. J. Kim, Y.-A. Song, and J. Han, "Nanofluidic concentration devices for biomolecules utilizing ion concentration polarization: Theory, fabrication, and applications," Chem. Soc. Rev. **39**, 912 (2010).
[53] T. A. Zangle, A. Mani, and J. G. Santiago, "Theory and experiments of concentration polarization and ion focusing at microchannel and nanochannel interfaces," Chem. Soc. Rev. **39**, 1014 (2010).